ELSEVIER

Strength of the lithosphere of the Galilean satellites

Karen Luttrell [*], David Sandwell

Scripps Institution of Oceanography, La Jolla, CA 92093-0225, USA

Received 10 June 2005; revised 19 January 2006

Abstract

Several approaches have been used to estimate the ice shell thickness on Callisto, Ganymede, and Europa. Here we develop a method for placing a strict lower bound on the thickness of the strong part of the shell (lithosphere) using measurements of topography. The minimal assumptions are that the strength of faults in the brittle lithosphere is controlled by lithostatic pressure according to Byerlee's law and the shell has relatively uniform density and thickness. Under these conditions, the topography of the ice provides a direct measure of the bending moment in the lithosphere. This topographic bending moment must be less than the saturation bending moment of the yield strength envelope derived from Byerlee's law. The model predicts that the topographic amplitude spectrum decreases as the square of the topographic wavelength. This explains why Europa is rugged at shorter wavelengths (∼10 km) but extremely smooth, and perhaps conforming to an equipotential surface, at longer wavelengths (>100 km). Previously compiled data on impact crater depth and diameter [Schenk, P.M., 2002. Nature 417, 419–421] on Europa show good agreement with the spectral decrease predicted by the model and require a lithosphere thicker than 2.5 km. A more realistic model, including a ductile lower lithosphere, requires a thickness greater than 3.5 km. Future measurements of topography in the 10–100 km wavelength band will provide tight constraints on lithospheric strength.
© 2006 Elsevier Inc. All rights reserved.

Keywords: Europa; Ganymede; Callisto; Ices; Tectonics

1. Introduction

Three of the four Galilean satellites of Jupiter have significant quantities of water and are referred to as icy satellites (Pappalardo et al., 1999; Showman and Malhotra, 1999). Galileo spacecraft magnetometer data from Europa indicate a near-surface conductive layer (Kivelson et al., 2000) suggesting that a liquid ocean lies beneath an ice shell. The thickness of the ice shell is of chief importance for the understanding of geologic processes on the Galilean satellites, the search for astrobiological activity on Europa, and the planning of future spacecraft missions. The ice shell is believed to be rheologically layered (Fig. 1a) consisting of a strong upper layer, or lithosphere, and possibly a convecting lower layer (Goldsby and Kohlstedt, 2001; McKinnon, 1999; Nimmo et al., 2003a). Here we investigate a new method for estimating the integrated strength of the lithosphere by measuring topographic moment.

The new strength estimates provide a strict lower bound on the thickness of the lithospheres of Callisto, Ganymede, and Europa although they do not provide an estimate of the total shell thickness of these satellites.

Ice shell thickness is usually estimated in one of three ways (Billings and Kattenhorn, 2005). The first approach uses models of heat transport along with estimates of internal heat generation to determine the thickness of the ice shell. Thermal studies on Europa yield total shell thicknesses ranging from 2–5 km (Thomson and Delaney, 2001) to 4 km (Ruiz, 1997) to 10–20 km (McKinnon, 1999) to 30 km (Wang and Stevenson, 2000). The second approach compares observed topography with the flexural response of a thin elastic plate to an assumed initial load to determine the thickness of the plate (Watts, 2001). For the terrestrial planets, the thickness of the elastic plate is about half of the total lithospheric thickness. Europa's elastic plate thickness has been estimated at 100–500 m (Williams and Greeley, 1998) to 4 and 6 km (Figueredo et al., 2002; Nimmo et al., 2003b) yielding total shell thickness of 15 km (Nimmo et al., 2003b). Effective elastic plate thickness estimates on

* Corresponding author. Fax: +1 858 534 2902.
  E-mail address: kluttrell@ucsd.edu (K. Luttrell).

2   *K. Luttrell, D. Sandwell / Icarus ••• (••••) •••–•••*

(a)

(b)
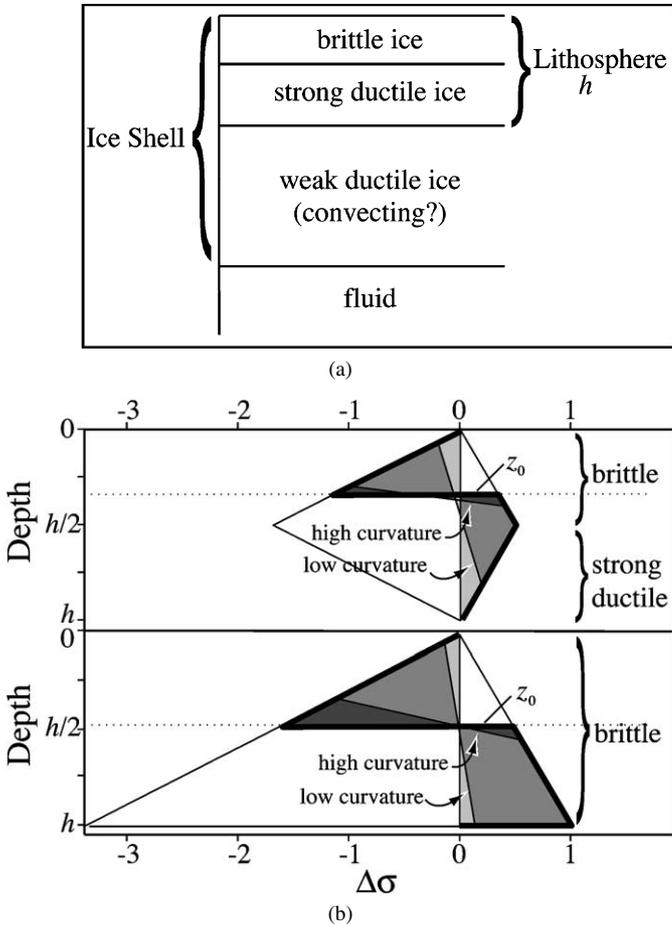
Fig. 1. (a) Ice shell consists of a strong lithosphere overlying a possibly-convecting weak ice layer. The lithosphere has a brittle upper layer and a strong ductile lower layer. (b) Yield strength envelope models for concave up bending. Mirrored model (above) represents a plausible lithosphere (Eq. (1)). Ice sheet model (below) represents the strongest possible lithosphere (Eq. (2)). Compressional deviatoric stress is negative, extensional stress is positive. Dotted line shows nodal plane depth z_0 for a moment-saturated plate, heavy black line shows stress state of a moment-saturated plate, and shaded sections indicate stress state for a plate with low and high curvatures.

Ganymede are 0.15–1.7 km (Nimmo and Pappalardo, 2004; Nimmo et al., 2002). A third approach to estimating shell thickness involves examining the morphologic transitions of impact craters and relating these to rheologic transitions at depth. Estimates of Europa's total shell thickness range from greater than 3–4 km (Turtle and Pierazzo, 2001) to 19–25 km (Schenk, 2002).

Here we develop a fourth approach to estimating the strength and minimum thickness of just the lithosphere. This involves comparing the bending moment needed to support topography with the maximum bending moment that the lithosphere is capable of supporting. Topography of satellites or planets having thin lithospheres can be supported either by a local compensation mechanism (e.g., Airy or Pratt) or by the strength of the lithosphere. On the terrestrial planets, compositional stratification enables a mix of compensation mechanisms so other information such as gravity and reflection seismology is needed to establish the dominant mechanism (Watts, 2001). However,

since the lithospheres of the Galilean satellites are largely homogeneous, lithospheric strength may be the dominant support mechanism. On Earth, studies of plate bending at subduction zones show that the critical measure of lithospheric strength is the topographic bending moment which can be calculated from the topography of the trench and outer rise (Goetze and Evans, 1979). The trench/outer rise topography would collapse if the overall strength of the lithosphere, or saturation bending moment, is less than the topographic bending moment (McAdoo et al., 1978). Thus measurements of topography provide a strict lower bound on lithospheric strength.

We use a similar approach to estimate the saturation bending moment of the lithosphere on the Galilean satellites. We assume that topography initially caused by large impact craters or tectonic processes induces stresses that exceed the strength of the lithosphere and have a bending moment greater than the long-term, saturation bending moment of the lithosphere. The lithosphere relaxes under the load to achieve stable topography in a state of moment saturation. We compare estimates of topographic bending moment derived from studies of impact craters (Schenk, 2002) to end-member models of lithospheric strength to determine a lower bound for the lithospheric thickness. These bounds are in agreement with flexural studies of Europa (e.g., Figueredo et al., 2002) and also provide insights into the lithospheric properties of Ganymede and Callisto.

An interesting feature of moment saturation analysis is that it predicts a particular form for the topographic spectrum. At wavelengths greater than the lithospheric thickness, the amplitude of the topography decreases as the square of the wavelength; this simple model explains why Europa appears smooth at large horizontal scales yet rough at small scales. At wavelengths less than the lithospheric thickness, the slope of the topography is limited by the angle of repose of the ice. The combined spectrum has a shape that depends only on the saturation bending moment. Using this spectrum we simulate the topography of Europa and compare artificial profiles with actual topographic profiles derived from stereo topography (Schenk and Pappalardo, 2004). We also convolve the synthetic topography with a series of averaging filters to investigate the practical sampling characteristics an altimeter mission would need in order to detect tidal fluctuations or variations in the equipotential surface (geoid) height.

2. Saturation bending moment and yield strength envelope models

When the lithosphere is subjected to a small bending moment it flexes with a curvature that is linearly related to the applied moment (Turcotte and Schubert, 2002). The thin elastic plate flexure model is only valid in this linear regime. As the applied moment is increased, stresses on the top and bottom of the lithosphere exceed the strength of the material and a plastic hinge develops (McAdoo et al., 1978). Eventually the lithosphere becomes moment-saturated so that the curvature of the hinge continues to increase without an increase in applied moment. At this point the thickness of the elastic core of the plate goes to zero (McNutt and Menard, 1982). The magnitude

of the saturation moment is a measure of the overall strength of the lithosphere. Moment saturation commonly occurs at ocean trenches on the Earth where lithosphere is permanently bent prior to subduction into the mantle (Levitt and Sandwell, 1995; McNutt and Menard, 1982). The nearly complete failure of the plate is evident as deeply penetrating normal faults that develop in the outer trench wall (Masson, 1991). Topographic profiles across the trench and outer rise provide a direct measure of the applied bending moment that can be compared with the rheological saturation bending moment (Brace and Kohlstedt, 1980; Goetze and Evans, 1979).

The strength of the lithospheric versus depth, or yield strength envelope, depends on pressure, temperature, and strain rate. In the upper lithosphere, strength is controlled primarily by the increase in lithostatic pressure with depth which inhibits sliding along preexisting fault planes according to Byerlee's law (Byerlee, 1978). As temperature increases in the lower part of the lithosphere, yielding occurs by ductile flow and strength decreases with depth (Goetze and Evans, 1979). While laboratory experiments have been partially successful in constraining the ductile rheology of the lower lithosphere (Kirby, 1983) the ultimate test for tenability of a rheologic model is whether the integrated yield strength is capable of supporting the observed trench/outer rise topography.

Here we apply the same concepts to the lithospheres of the icy Galilean satellites. Cold dry ice undergoes brittle yielding similar to that of the terrestrial lithosphere. Beeman et al. (1988) has conducted frictional sliding experiments on very cold (77–115 K) saw-cut ice cores and established a frictional sliding relationship that is specific to ice with a coefficient of friction value of 0.69 (i.e., Byerlee's law for ice). The strength of the lower ductile portion of the lithosphere is highly uncertain (Goldsby and Kohlstedt, 2001) and depends on unknown parameters such as grain size, thermal gradient, strain rate, and activation energy. Given this uncertainty, we consider two cases. In the first case (mirrored model), the strength of the lower ductile layer decreases linearly with depth and mirrors the strength of upper brittle layer (Fig. 1b). The yield stress envelope for this case is (Brace and Kohlstedt, 1980; Watts, 2001)

$$\Delta\sigma_{\text{comp}} = \begin{cases} -C\rho gz, & z < h/2, \\ -C\rho g(h-z), & z > h/2, \end{cases}$$

$$\Delta\sigma_{\text{ten}} = \begin{cases} \alpha C\rho gz, & z < h/2, \\ \alpha C\rho g(h-z), & z > h/2, \end{cases} \quad (1)$$

where ρ is the density of the ice (980 kg m^{-3}), g is gravity (1.3 m s^{-2}), h is the thickness of the lithosphere, and the dimensionless factors $C = 2.6$ and $\alpha = 0.3$ are constants resulting

from our use of Byerlee's law for ice (compare with $C = 4$ and $\alpha = 0.2$ for most types of rock; e.g., Watts, 2001). In the second case (ice sheet model), strength increases with depth in the brittle layer and abruptly goes to zero as one would find for a brittle ice sheet floating on a liquid ocean. This case has a yield strength envelope given by

$$\Delta\sigma_{\text{comp}} = -C\rho gz,$$

$$\Delta\sigma_{\text{ten}} = \alpha C\rho gz. \quad (2)$$

For a prescribed lithospheric thickness h, the ice sheet model will support the maximum topographic moment. Thus given a topographic moment, this model provides an absolute lower bound on lithospheric thickness.

In addition to the shape of the yield strength envelope, the saturation bending moment also depends on the sign of the curvature—whether the lithosphere is flexed concave up or concave down. When the lithosphere is flexed concave down, such as at a subduction zone, the top portion of the lithosphere undergoes tension (weaker) while the bottom part undergoes compression. In concave up flexure, such as under a seamount, the top portion of the lithosphere is in compression (stronger); this usually results in a larger saturation bending moment due to the shape of the strength envelope. Saturation moment is found by integrating yield strength times moment arm over depth (Eq. (3)):

$$M_s = \int_0^h \Delta\sigma_{\text{yield}}(z - z_0)\, \mathrm{d}z. \quad (3)$$

For concave up bending, $\Delta\sigma_{\text{yield}} = \Delta\sigma_{\text{comp}}$ above the nodal plane, or neutral unstrained surface, and $\Delta\sigma_{\text{yield}} = \Delta\sigma_{\text{ten}}$ below the nodal plane. For concave down bending the roles of tensile yield stress and compressive yield stress are reversed. The moment arm $(z - z_0)$ is the distance above or below the nodal plane. We assume there is no net horizontal force on the lithosphere so the nodal depth, z_0, is found by requiring the integral of stress over depth equal zero (Eq. (4)):

$$\int_0^{z_0} \Delta\sigma_{\text{yield}}\, \mathrm{d}z + \int_{z_0}^h \Delta\sigma_{\text{yield}}\, \mathrm{d}z = 0. \quad (4)$$

The nodal depth will depend on both the sign and magnitude of the lithosphere curvature. At low curvature, z_0 will be close to $h/2$. As curvature increases, z_0 will drift away from $h/2$ to reach an extreme value when the lithosphere reaches moment saturation. The relation between saturation nodal depth and h, given in Table 1, depends on both the

Table 1
Depth to nodal plane z_0 in moment-saturated plate as a function of plate thickness h for four different cases

	Concave up	Concave down
Mirrored model (brittle and strong ductile)	$z_0 = \sqrt{\frac{\alpha}{2(1+\alpha)}}\, h = 0.34h$	$z_0 = \left[1 - \sqrt{\frac{\alpha}{2(1+\alpha)}}\right] h = 0.66h$
Ice sheet model (brittle only)	$z_0 = \sqrt{\frac{\alpha}{1+\alpha}}\, h = 0.48h$	$z_0 = \sqrt{\frac{1}{1+\alpha}}\, h = 0.88h$

Table 2
Dimensionless geometric factor γ, depending only on the constants $C = 2.6$ and $\alpha = 0.3$ from Byerlee's law for ice

	Concave up	Concave down
Mirrored	$\gamma = C\left[\frac{1}{8}\alpha - \frac{1}{6\sqrt{2}}\frac{\alpha^{3/2}}{(1+\alpha)^{1/2}}\right] = 0.053$	$\gamma = -C\left[\frac{1}{8}\alpha - \frac{1}{6\sqrt{2}}\frac{\alpha^{3/2}}{(1+\alpha)^{1/2}}\right] = -0.053$
Ice sheet	$\gamma = C\left[\frac{1}{3}\alpha - \frac{1}{3}\frac{\alpha^{3/2}}{(1+\alpha)^{1/2}}\right] = 0.135$	$\gamma = -C\left[\frac{1}{3} - \frac{1}{3}\frac{1}{(1+\alpha)^{1/2}}\right] = -0.107$

geometry of the yield strength envelope and the sign of the curvature. For a moment-saturated lithosphere with ice sheet yield strength envelope, the location of z_0 is highly asymmetric with respect to bending direction, located near the center of the concave up lithosphere and near the bottom of the concave down lithosphere. A moment-saturated lithosphere with mirrored yield strength envelope has a z_0 location that is symmetric with regard to the direction of bending located significantly away from the center of the lithosphere.

Having identified two yield strength envelopes of interest and their four possible saturation nodal depths, we calculate the saturation bending moment using Eq. (3). For all cases above the saturation moment is proportional to the lithostatic pressure $\rho g h$ times lithosphere thickness squared times a dimensionless factor γ that depends on the shape of the yield strength envelope and the sign of lithosphere curvature (Eq. (5)):

$$M_s = \gamma \rho g h^3. \tag{5}$$

The geometric factor γ for the four cases is given in Table 2. For an ice sheet model of thickness h, the magnitude of the saturation bending moment is greater for concave up bending than for concave down bending because the lithosphere is stronger in compression than in tension and brittle strength increases dramatically with depth. For a mirrored model of the same thickness, the magnitude of the saturation moment is independent of bending direction and is about half the value of the concave down ice sheet model.

3. Maximum observed topographic bending moment

A unique feature of the Galilean satellites, and in particular Europa, is that the density of the icy shell is nearly uniform ($<5\%$ density variation) (Schenk and Pappalardo, 2004). On the Earth and other terrestrial planets, the lithosphere is comprised of a lower density crust underlain by a higher density mantle. Since both layers are imbedded with a relatively strong elastic layer, long-wavelength topography can be supported by Airy compensation. On Europa, topography at wavelengths greater than about 1000 km could be maintained over long timescales by significant shell-thickness variations if the rheology of the shell is non-Newtonian (Nimmo, 2004). At wavelengths shorter than about 100 km, however, the horizontal pressure gradients between the weak ductile ice layer at the base of the shell and the liquid water below will cause the base of the shell to flatten on relatively short timescales (Nimmo, 2004; O'Brien et al., 2002; Stevenson, 2000). These properties have important consequences for how topography is physically supported. Because Airy compensation is unlikely on the Galilean satellites, especially over horizontal length scales less than

100 km (Nimmo, 2004), topography must be supported by an alternative mechanism. It is possible to support a few hundred meters of topography through Pratt compensation if the shell thickness is >15 km (Schenk and Pappalardo, 2004). For this analysis, however, we consider the integrated strength of the lithosphere as the primary support mechanism so that we may explore the possibility of thinner (<10 km) shells and put an absolute lower bound on shell thickness.

As shown in many investigations on Earth, the appropriate parameter to characterize strength of a plate is the saturation bending moment which is the integral of the yield strength over depth times the distance to the flexural nodal plane (Goetze and Evans, 1979) (see Section 2). Bending moment can also be measured from the observed topography without knowledge of the plate material or yield strength profile. In the case of trench flexure, the bending moment depends on the integral of the vertical topographic load $g\rho w(x)$ times the moment arm $(x - x_0)$,

$$M(x_0) = g \int_{x_0}^{\infty} \rho w(x)(x - x_0)\,\mathrm{d}x, \tag{6}$$

where x_0 is the first zero crossing outboard of the trench axis. This is a simple integration of topography with no unknown model parameters; the results depend only on the location of the zero crossing.

We show next that the topographic spectrum of the Galilean satellites can be used to estimate the bending moment of the lithosphere. Conversely, given the saturation bending moment of the lithosphere (Section 2), one can derive an upper bound on the topographic spectrum. In the case of real Galilean topography there may not be a dominant flexural wavelength as in the case of trench flexure so we first consider the case of arbitrary topography to develop a general expression for the moment. We then consider the case of cylindrically symmetric topography to calculate an approximate moment associated with impact craters of a given depth and diameter (Schenk, 2002).

Consider an event such as a meteorite impact or other tectonic process that instantaneously creates topography $a(\mathbf{x})$ with a bending moment greater than the saturation bending moment of the lithosphere (Fig. 2a). Over geologic timescales the lithosphere will relax by an amount $w(\mathbf{x})$ to support this initial topographic load. The final topography, which can be observed, will be the sum of the initial topography and the plate deflection $t(\mathbf{x}) = a(\mathbf{x}) + w(\mathbf{x})$ (Fig. 2b). The standard thin-plate moment balance equation is used to calculate the plate deflection from the applied topographic load (e.g., Turcotte and Schubert, 2002):

$$-\nabla^2 M(\mathbf{x}) + \rho g w(\mathbf{x}) = -\rho g a(\mathbf{x}), \tag{7}$$
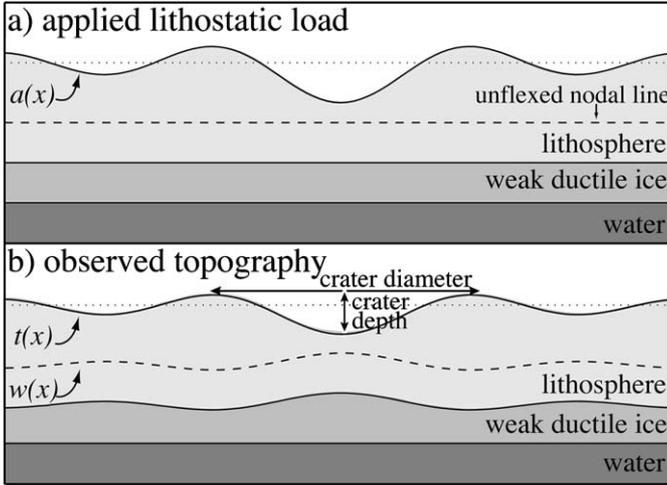
Fig. 2. Response of the lithosphere to an initial topographic load. (a) Topographic load $a(x)$ applied to an initially unbent plate (dashed line represents nodal plane). (b) Observed topography $t(x)$ following relaxation is the sum of the applied topography $a(x)$ and the bending response $w(x)$.

where M is the bending moment and ρ is the density of the ice. Note that this analysis does not assume a linear relationship between moment and curvature as in the case of elastic plate flexure. Because the base of the ice shell is flat on long timescales there is no contribution to the restoring from the ice/water interface. The solution to Eq. (7) in the Fourier domain is

$$M(\mathbf{k}) = -\frac{\rho g}{(2\pi |\mathbf{k}|)^2} T(\mathbf{k}), \qquad (8)$$

where $T(\mathbf{k})$ is topography in the wavenumber domain, $k_x = 1/\lambda_x$, $k_y = 1/\lambda_y$, and $|\mathbf{k}| = \sqrt{k_x^2 + k_y^2}$. This relationship between bending moment and observed topography is independent of rheology and only depends on the gravitational restoring force. This is directly analogous to Eq. (6) where the trench/outer rise topography is used to estimate bending moment.

Equation (8) has some exciting implications. First, if one had complete topographic measurements of the icy satellites, then the bending moment could be calculated directly without having to assume values for unknown parameters. Moreover, if the lithosphere has a spectrally uniform saturation bending moment, then the topographic spectrum must decrease as the wavelength squared. This could explain why Europa appears smooth on global scales yet quite rugged on local scales ($\sim$10 km). Second, at intermediate and perhaps long wavelengths, the topography of Europa may conform to an equipotential surface of gravity so topographic measurements could provide direct measurements of geoid height. These could be used to search for the gravitational signatures of volcanoes at the bottom of Europa's ocean, for example.

We test the saturation moment prediction of Eq. (8) through a comparison of impact crater topography on the icy Galilean satellites (Schenk, 2002). Craters shapes are highly variable so we approximate their topography $t(r)$ (Eq. (9)) using a radially

symmetric Bessel function of the first kind (Fig. 2)

$$t(r) = A_0 J_0(2\pi k_0 r), \qquad (9)$$

where r is radial distance, k_0 is a characteristic radial wavenumber and A_0 is the central amplitude. Taking the Hankel transform of Eq. (9), substituting into Eq. (8), and then taking the inverse Hankel transform we obtain the topographic bending moment as a function of radius (Eq. (10)):

$$M(r) = -\frac{\rho g}{(2\pi k_0)^2} A_0 J_0(2\pi k_0 r). \qquad (10)$$

The maximum bending moment magnitude occurs at the center of the crater where $J_0(0) = 1$, and has a value given by

$$M_{\max} = \frac{\rho g}{(2\pi k_0)^2} A_0. \qquad (11)$$

We follow the convention of Schenk (2002) to define crater depth as the vertical distance between the central minimum and the first maximum and crater diameter as the horizontal distance between the two maxima (Eq. (12)):

$$\text{depth} = 1.4028 A_0,$$
$$\text{diameter} = \frac{3.8317}{\pi k_0}. \qquad (12)$$

Combining Eqs. (11) and (12) provides a relationship between crater depth, crater diameter, and maximum bending moment:

$$\text{depth} = 20.5958 \left(\frac{4 M_{\max}}{\rho g} \right) \frac{1}{\text{diameter}^2}. \qquad (13)$$

Although a single wavenumber Bessel function may seem like a crude approximation to the shape of the topography of an impact crater, we have found through simulations that the topographic moment is dominated by the amplitude of the longest wavelength component. In other words, adding complicated short wavelength topographic structure will have negligible effect on maximum moment.

4. An upper bound on the topographic spectrum from the yield strength envelope

Before applying these concepts to the icy Galilean satellites it is instructive to test the approach using subduction zone data on the Earth. Levitt and Sandwell (1995) estimated topographic moment across 37 trench and outer rise flexures. Rather than numerically integrate the noisy topographic data, they first fit the topographic profiles with a thin elastic plate flexure model and then integrated the best-fit model to estimate the moment (Eq. (6)). Their results (Fig. 3a) show that the topographic moment increases nearly linearly with lithospheric age, which is explained by a combination of thickening and strengthening of the lithosphere as it cools. The measured moments are then compared to the saturation bending moment computed from a yield strength envelope consisting of a brittle layer following Byerlee's law and a power law ductile flow using a half-space cooling model (Goetze and Evans, 1979). In all but three of the cases, the topographic moment of the trench is less than the model saturation bending moment suggesting that the cooling model and rheology are in accordance with the data.
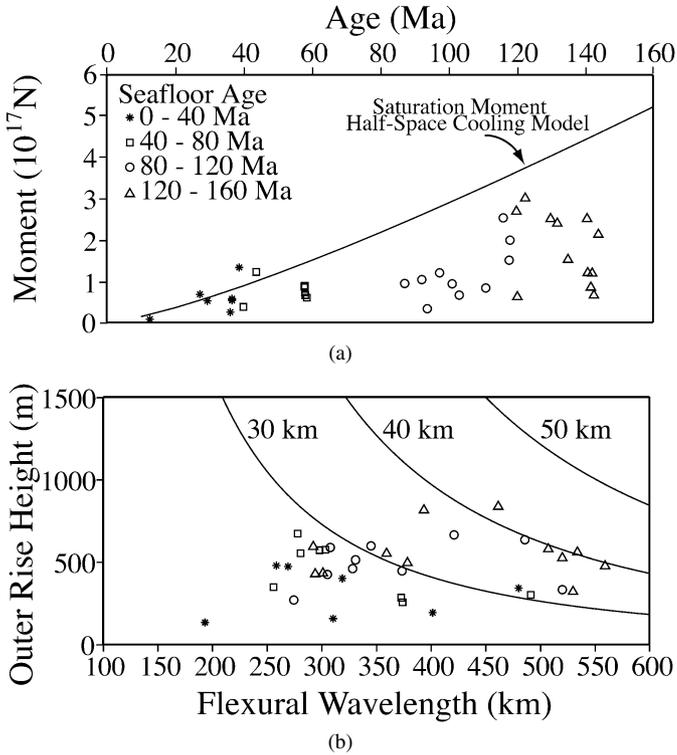
Fig. 3. (a) Topographic moment (symbols) across 37 trench and outer rise profiles on the Earth (Levitt and Sandwell, 1995). Saturation moment (solid curve), based on a yield strength envelope model, increases with age as the lithosphere cools and thickens. All but three of the observed moments fall below the saturation moment curve. (b) Outer rise height and flexural wavelength of the same 37 profiles. Saturation moment contours (solid curves) for a lithosphere with mirrored yield strength envelope (Fig. 1b). Saturation moment and lithospheric thickness increase with age, as expected for Earth.

Fig. 4. Impact crater depth versus crater diameter (after Schenk, 2002). Dotted line shows 17° slope limit for small diameter craters. Solid curves are crater depth predicted by a moment-saturated lithosphere having the ice sheet yield-strength envelope. Large diameter craters on (a) Callisto and (b) Ganymede are supported by a lithosphere thickness ranging from 2–10 km. Large diameter craters on (c) Europa are supported by a minimum 2.5 km thick lithosphere. The more realistic mirrored model requires a minimum 3.5 km thick lithosphere.

Fig. 3b shows the trench measurements of outer rise height (analogous to crater depth) versus flexural wavelength (analogous to crater diameter), $\lambda = \sqrt{2}\pi\alpha = 1/k$ where α is the flexural parameter (Watts, 2001). The model curves are calculated by combining Eqs. (5) and (8) to relate lithosphere thickness h to wavelength $1/k$ using the γ value of a mirrored yield strength envelope. While the mirrored model is a crude approximation to the actual Earth, it provides an informative check on a well-understood data set. The comparisons show that older lithosphere (triangles and circles) generally require a thicker plate than younger lithosphere (asterisks and squares). The thicknesses are in good agreement with the flexural modeling estimates (Levitt and Sandwell, 1995). The success of this simple formulation on Earth data suggests it can be applied to the icy satellites where topographic information is far more limited.

To apply these concepts to the icy Galilean satellites we need to examine topographic features that are moment-saturated and have a dominant characteristic wavelength. The best published data set for this purpose is impact crater depth (rim to floor) versus diameter (rim to rim) (Schenk, 2002). For small craters (<5 km in diameter) there is a nearly linear relationship between crater depth and diameter that is consistent with a maximum ice slope of 17°. Schenk (2002) interpreted all of these small craters as having a simple morphology suggesting that they did not penetrate the lithosphere. Larger craters (>10 km) have more complex morphology suggesting they penetrated partially (complex crater) or entirely through the lithosphere (central pit or dome crater) (Schenk, 2002).

We propose that crater depth is limited by the minimum of two competing mechanisms—the 17° maximum slope and the saturation bending moment. Fig. 4 compares impact crater data from Callisto, Ganymede, and Europa with contours of lithosphere thickness calculated by combining Eqs. (5) and (13) using $\gamma = 0.135$, the value of an ice sheet yield strength envelope with concave up bending. For Callisto and Ganymede (Figs. 4a and 4b), there is no clear upper bound on the crater data; rather a range of thickness 2–10 km fits the data. The lack of a single thickness for the upper bound can be explained in three ways: (i) the true thickness is greater than 10 km and the crater topographies do not represent moment saturation; (ii) the thickness varies with location; (iii) the thickness has changed with time so some craters formed while the lithosphere was thick while others formed while the lithosphere was thin. Note that the Earth data show a similar dispersion that is due to thickening of the lithosphere with age.

The relationship between crater depth and diameter is notably different on Europa (Fig. 4c). Crater depth peaks at a diameter of about 8 km and then falls roughly following the 2-km thick lithosphere. The peak in the observed crater depth

(∼800 m) is not as large as the model peak (∼1500 m) possibly because the thin plate approximation breaks down in this wavelength band. Nevertheless there is good agreement between these simple models and the available data suggesting Europa's lithosphere is no thinner than 2.5 km. The more realistic mirrored model requires a thickness greater than 3.5 km. The most important feature of this comparison is the decreasing crater depth with increasing diameter, especially for diameters >20 km. This spectral decrease is consistent with the apparent blue topographic spectrum of Europa; it appears smooth at intermediate wavelengths (100–1000 km) but quite rough at smaller scales (2–20 km). In contrast, most rocky planets, e.g., Venus, Earth, and Mars have a red topographic spectrum (Bills and Lemoine, 1995).

5. Discussion

One of the interesting predictions of this method is that it places an upper bound on the topographic spectrum of Europa. This has important tectonic and practical consequences. From a tectonics perspective, any long wavelength topography that exceeds this bound (e.g., Murias Chaos "Mitten," Figueredo et al., 2002) must be supported either by local compensation, due to nonuniform tidal heating (Ojakangas and Stevenson, 1989), or by convective activity in the weak ductile ice beneath the lithosphere. From a practical perspective, the upper bound on the amplitude spectrum can be used to design topographic sampling strategies for measuring tides, long-wavelength topography due to shell thickness variations, and geoid height in regions not dominated by Airy-compensated topography.

Existing topographic grids are not large enough for accurate spectral analysis and also have long-wavelength errors due to the inaccuracies in the stereo-DEM generation process. Moreover, spectra produced from a 1D profile do not accurately represent the true 2D spectrum, especially when the spectrum is blue. Therefore we explore the tectonic and practical consequences of the predicted topographic spectrum by generating synthetic topography that has bending moment less than or equal to the saturation moment observed in Fig. 4c and surface slopes less than or equal to 17°. This is accomplished using a statistical approach by first generating random topography uniformly distributed in wavenumber domain, and then forcing it to conform to the model spectrum of Fig. 4c.

An important issue on Europa is whether or not density variations within the shell are required to explain the observed topography in the 20–100 km wavelength band. Schenk and Pappalardo (2004) have proposed that intermediate-scale topography (∼20–100 km) must be supported by Pratt isostasy since the bottom surface of the ice shell will become flat, erasing any perturbations, over a relatively short timescale (10^5 years) (Nimmo, 2004; Stevenson, 2000) making Airy isostasy impossible. They in turn use this argument to rule out the possibility of a thin-shelled Europa. Here we show that Pratt isostasy is not required, although still possible, because the 20 km-scale topography could be supported by the strength of the shell. Fig. 5a shows a 200 km long profile of
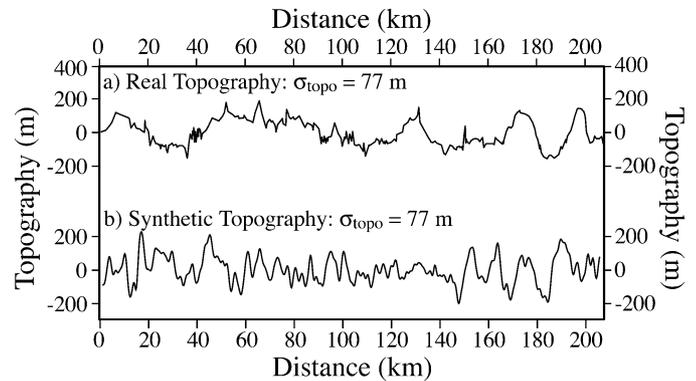
Fig. 5. (a) Topographic profile from Conamara Chaos region of Europa with standard deviation 77 m and maximum slope 16° (Schenk and Pappalardo, 2004). (b) Synthetically derived topography with standard deviation 77 m and maximum slope 17°. Maximum moment along this profile corresponds to a 3-km thick plate.

topography on Europa taken from the Conamara Chaos region of relatively large amplitude topography. The topography data comes from a stereo-controlled photoclinometry Digital Elevation Model produced by Schenk and Pappalardo (2004) and has a standard deviation of 77 m and a maximum slope of 16°. Fig. 5b shows a profile taken from our synthetically derived topography, bounded by a 17° slope and the saturation moment corresponding to a 3 km thick ice sheet model lithosphere. The two profiles have similar peak to trough amplitude and visually similar spectrum. This analysis suggests that Pratt isostasy is not required to explain the 20 km-scale topography since it can also be supported by the strength of the lithosphere. However, if one were to observe topography outside the saturation moment limit, then another mechanism of support such as local isostasy or convection would be needed.

A second important issue on Europa is how best to measure the long-wavelength topographic variations due to tides, shell thickness variations, and geoid height. Proposed instruments include a laser altimeter profiler, which has excellent absolute height accuracy but poor spatial sampling, and a synthetic aperture radar interferometer that can measure a wide swath but has inferior height accuracy. Tidal fluctuations are estimated to be as large as 30 m (Greenberg et al., 2002; Moore and Schubert, 2000) on a global scale (∼10,000 km wavelength). To learn something new about generation of heat by tidal dissipation will require understanding the phase lag of the tide relative to the gravitational forcing functions so perhaps a 1-m accuracy will be needed. Another possible feature of interest is the shape of the planet's equipotential surface, or "geoid," caused by mass variations at the floor of Europa's ocean. If the ocean and ice shell are in isostatic equilibrium at long wavelengths (>200 km), it may be possible to measure the height of the geoid with an altimeter. Altimeters have been used to measure the geoid over areas of permanent ice cover on the Earth (Laxon and McAdoo, 1994). The expected geoid signal can be crudely estimated by placing a large uncompensated volcano at the base of a 100 km deep ocean. A volcano having mass comparable to Mauna Loa (Hawaii) or Haemus Montes

or Euboea Montes (Io) (Schenk and Bulmer, 1998) produces a geoid bump 1–10 m tall and 400 km across. Thus both the tidal signal and the geoid signal are about 100 times smaller than the RMS of the topography of Europa so the question is—what is the best way to sample and average the topography to extract the small-amplitude long-wavelength signals from the shorter-wavelength topographic "noise"?

To assess the possibility of measuring topography to a 1 m vertical accuracy at long wavelengths, we investigate the end member strategies for sampling and averaging of a synthetic topography grid with the model spectrum of Fig. 4c. (Note the tidal fluctuations can also be detected at crossover points of altimeter profiles and our analysis does not consider this type of sampling.) The laser altimeter has 200 m diameter footprint and 200 m along-track sampling. The swath altimeter has the same 200-m by 200-m resolution but samples a swath 10 km wide (i.e., 50 pixels wide). Of course, the swath data can be averaged across-track to reduce the topographic noise by a factor of ∼5 but this still does not achieve the desired accuracy of 1 m. Additional noise reduction is gained by Gaussian-averaging the profiles along the satellite track. Fig. 6 shows the level of vertical accuracy achieved by the two instruments by along-track averaging. The laser-altimeter achieves the 1-m threshold at an averaging wavelength of 1000 km. This sampling is adequate for resolving the 10,000-km wavelength tides but inadequate for detecting the geoid expression of a large ocean floor volcano. The swath altimeter achieves the 1-m threshold at a wavelength of 700 km. In this case the tidal signal is resolved but only the longer-wavelength components of the ocean floor volcano could be resolved. It must be emphasized that these results rely on the assumption that all topography is supported by the strength of the lithosphere. This assumption is likely to be invalid at some points on Europa's surface. Any long-wavelength topography having amplitude >1 m that is supported by an Airy, Pratt, or convective mechanism will mask the tidal and geoid signals. In this case a crossover analysis will be needed to extract the tidal signal and the geoid signal will be immeasurable.
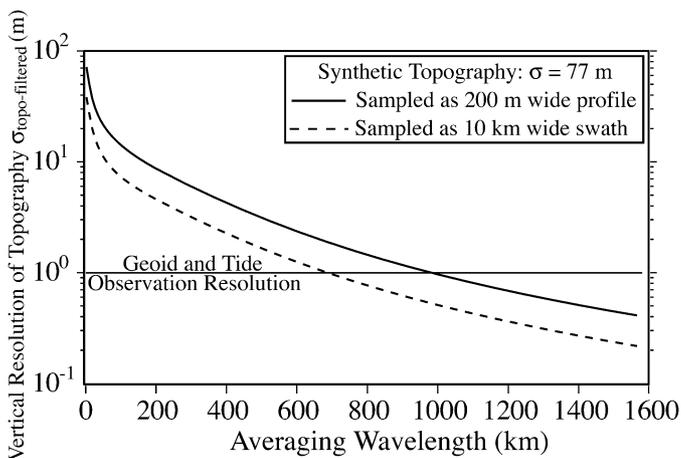
Fig. 6. Vertical accuracy of sampled topography versus wavelength of averaging. Solid and dashed lines are for profile instrument (200 m width), and swath instrument (10 km width), respectively. A 1 m vertical resolution is required to study geoid and tide variations.

6. Conclusions

Saturation moment analysis is a useful companion to existing methods of estimating lithosphere thickness. Rather than relying on estimates of specific material properties that are poorly constrained, it instead makes a more fundamental estimation of the first-order behavior of the general material by selecting the shape of the lithosphere's yield strength envelope. By using the strongest possible yield strength envelope, an absolute lower bound on lithospheric thickness can be established. Moment analysis also gives a more robust estimate of lithosphere thickness since it simultaneously incorporates multiple features of multiple length scales to constrain its estimates rather than a single feature of a single scale.

Craters of large diameter (> ∼10 km) on Callisto and Ganymede exhibit multiple topographic moments, as do trenches at subduction zones on Earth, indicating a range of lithosphere thicknesses. We conclude that lithosphere thickness on these satellites in the vicinity of these impact craters either (i) varies in the range of a few km to ∼10 km or (ii) is everywhere thicker than 10 km (or some combination of the two). These estimates are significantly larger than previous estimates of effective elastic plate thickness. Craters on Europa coincide with a single observed topographic moment for large craters (diameter > ∼6 km) suggesting a lithosphere thickness greater than 2.5 km in the vicinity of the craters. This estimate lies between the thinner effective elastic thickness estimates of Williams and Greeley (1998) and thicker estimates of Figueredo et al. (2002) and Nimmo et al. (2003b).

The impact crater depth/diameter relationship on Europa is consistent with a moment saturation model having a blue spectrum. This model explains why Europa appears smoother at long wavelengths than it does at short wavelengths. This spectrum can be used to statistically create synthetic topography grids much larger than the DEMs available from current data. Simulation of topography with this spectrum reveals that observed chaos topography can be supported by the strength of the lithosphere and do not require Pratt isostasy as a mechanism of support as has been suggested. Large synthetic topography grids allow us to examine intermediate wavelength characteristics and consider possible sampling strategies for an altimeter at Europa. Observation of geoid height and new understanding of tides requires 1 m of vertical resolution unobscured by small-scale topography. A 10 km swath instrument would require along track averaging of 700 km to achieve this resolution and a 200 m spot profiling instrument would require along track averaging on the order of 1000 km.

References

Beeman, M., Durham, W.B., Kirby, S.H., 1988. Friction of ice. J. Geophys. Res. 93, 7625–7633.

Billings, S.E., Kattenhorn, S.A., 2005. The great thickness debate: Ice shell thickness models for Europa and comparisons with estimates based on flexure at ridges. Icarus 177, 397–412.

Bills, B.G., Lemoine, F.G., 1995. Gravitational and topographic isotropy of the Earth, Moon, Mars, and Venus. J. Geophys. Res. 100, 26275–26295.

Brace, W.F., Kohlstedt, D.L., 1980. Limits on lithospheric stress imposed by laboratory experiments. J. Geophys. Res. 85, 6248–6252.

Byerlee, J., 1978. Friction of rocks. Pure Appl. Geophys. 116, 615–626.

Figueredo, P.H., Chuang, F.C., Rathbun, J., Kirk, R.L., Greeley, R., 2002. Geology and origin of Europa's "Mitten" feature (Murias Chaos). J. Geophys. Res. 107, doi:10.1029/2001JE001591.

Goetze, C., Evans, B., 1979. Stress and temperature in the bending lithosphere as constrained by experimental rock mechanics. Geophys. J. R. Astron. Soc. 59, 463–478.

Goldsby, D.L., Kohlstedt, D.L., 2001. Superplastic deformation of ice: Experimental observations. J. Geophys. Res. 106, 11017–11030.

Greenberg, R., Geissler, P., Hoppa, G., Tufts, B.R., 2002. Tidal-tectonic processes and their implications for the character of Europa's icy crust. Rev. Geophys. 40, doi:10.1029/2000RG000096.

Kirby, S.H., 1983. Rheology of the lithosphere. Rev. Geophys. 21, 1458–1487.

Kivelson, M.G., Khurana, K.K., Russell, C.T., Volwerk, M., Walker, R.J., Zimmer, C., 2000. Galileo magnetometer measurements: A stronger case for a subsurface ocean at Europa. Science 289, 1340–1343.

Laxon, S., McAdoo, D., 1994. Arctic-ocean gravity-field derived from ERS-1 satellite altimetry. Science 265, 621–624.

Levitt, D.A., Sandwell, D.T., 1995. Lithospheric bending at subduction zones based on depth soundings and satellite gravity. J. Geophys. Res. 100, 379–400.

Masson, D.G., 1991. Fault patterns at outer trench walls. Mar. Geophys. Res. 13, 209–225.

McAdoo, D.C., Caldwell, J.G., Turcotte, D.L., 1978. Elastic-perfectly plastic bending of lithosphere under generalized loading with application to Kuril trench. Geophys. J. R. Astron. Soc. 54, 11–26.

McKinnon, W.B., 1999. Convective instability in Europa's floating ice shell. Geophys. Res. Lett. 26, 951–954.

McNutt, M.K., Menard, H.W., 1982. Constraints on yield strength in the oceanic lithosphere derived from observations of flexure. Geophys. J. R. Astron. Soc. 71, 363–394.

Moore, W.B., Schubert, G., 2000. The tidal response of Europa. Icarus 147, 317–319.

Nimmo, F., 2004. Non-Newtonian topographic relaxation on Europa. Icarus 168, 205–208.

Nimmo, F., Pappalardo, R.T., 2004. Furrow flexure and ancient heat flux on Ganymede. Geophys. Res. Lett. 31, doi:10.1029/2004GL020763.

Nimmo, F., Pappalardo, R.T., Giese, B., 2002. Effective elastic thickness and heat flux estimates on Ganymede. Geophys. Res. Lett. 29, doi:10.1029/2001GL013976.

Nimmo, F., Pappalardo, R.T., Giese, B., 2003a. On the origins of band topography, Europa. Icarus 166, 21–32.

Nimmo, F., Giese, B., Pappalardo, R.T., 2003b. Estimates of Europa's ice shell thickness from elastically-supported topography. Geophys. Res. Lett. 30, doi:10.1029/2002GL016660.

O'Brien, D.P., Geissler, P., Greenberg, R., 2002. A melt-through model for chaos formation on Europa. Icarus 156, 152–161.

Ojakangas, G.W., Stevenson, D.J., 1989. Thermal state of an ice shell on Europa. Icarus 81, 220–241.

Pappalardo, R.T., Belton, M.J.S., Breneman, H.H., Carr, M.H., Chapman, C.R., Collins, G.C., Denk, T., Fagents, S., Geissler, P.E., Giese, B., Greeley, R., Greenberg, R., Head, J.W., Helfenstein, P., Hoppa, G., Kadel, S.D., Klaasen, K.P., Klemaszewski, J.E., Magee, K., McEwen, A.S., Moore, J.M., Moore, W.B., Neukum, G., Phillips, C.B., Prockter, L.M., Schubert, G., Senske, D.A., Sullivan, R.J., Tufts, B.R., Turtle, E.P., Wagner, R., Williams, K.K., 1999. Does Europa have a subsurface ocean? Evaluation of the geological evidence. J. Geophys. Res. 104, 24015–24055.

Ruiz, J., 1997. Onset of convection, heat flow and thickness of the Europa's ice shell. Earth Moon Planets 77, 99–104.

Schenk, P.M., 2002. Thickness constraints on the icy shells of the Galilean satellites from a comparison of crater shapes. Nature 417, 419–421.

Schenk, P.M., Bulmer, M.H., 1998. Origin of mountains on Io by thrust faulting and large-scale mass movements. Science 279, 1514–1517.

Schenk, P.M., Pappalardo, R.T., 2004. Topographic variations in chaos on Europa: Implications for diapiric formation. Geophys. Res. Lett. 31.

Showman, A.P., Malhotra, R., 1999. The Galilean satellites. Science 286, 77–84.

Stevenson, D.J., 2000. Limits on the variation of thickness of Europa's ice shell. Lunar Planet. Sci. 31. Abstract 1506.

Thomson, R.E., Delaney, J.R., 2001. Evidence for a weakly stratified Europan ocean sustained by seafloor heat flux. J. Geophys. Res. 106, 12355–12365.

Turcotte, D.L., Schubert, G., 2002. Geodynamics. Cambridge Univ. Press, New York.

Turtle, E.P., Pierazzo, E., 2001. Thickness of a European ice shell from impact crater simulations. Science 294, 1326–1328.

Wang, H., Stevenson, D.J., 2000. Convection and internal melting of Europa's ice shell. Lunar Planet. Sci. 31. Abstract 1293.

Watts, A.B., 2001. Isostasy and Flexure of the Lithosphere. Cambridge Univ. Press, New York.

Williams, K.K., Greeley, R., 1998. Estimates of ice thickness in the Conamara Chaos region of Europa. Geophys. Res. Lett. 25, 4273–4276.